Journal of Magnetism and Magnetic Materials 475 (2019) 429–435

Contents lists available at ScienceDirect

Journal of Magnetism and Magnetic Materials

journal homepage: www.elsevier.com/locate/jmmm

Research articles

Mn-Zn ferrite nanoparticles coated with mesoporous silica as core material for heat-triggered release of therapeutic agents

Janja Stergar[a,b], Zdeněk Jirák[a], Pavel Veverka[a], Lenka Kubíčková[a,c], Tomáš Vrba[a,d], Jarmila Kuličková[a], Karel Knížek[a], Florence Porcher[e], Jaroslav Kohout[c], Ondřej Kaman[a,*]

[a] Institute of Physics, Czech Academy of Sciences, Cukrovarnická 10, 162 00 Praha 6, Czech Republic
[b] University of Maribor, Faculty of Medicine, Taborska ulica 8, SI-2000 Maribor, Slovenia
[c] Faculty of Mathematics and Physics, Charles University, 180 00 Praha 8, Czech Republic
[d] University of Chemistry and Technology Prague, Department of Analytical Chemistry, Technická 5, 166 28 Prague 6, Czech Republic
[e] Lab Leon Brillouin, CEA Saclay, F-91191 Gif Sur Yvette, France

ARTICLE INFO

Keywords:
Magnetic nanoparticles
Hydrothermal synthesis
Spinel
Porosimetry
Drug loading
Cation distribution

ABSTRACT

Hydrothermal synthesis was employed to prepare three samples of Mn-Zn ferrite nanoparticles with the mean size of crystallites of 12–14 nm, whose compositions were accurately determined by X-ray fluorescence spectroscopy to $Mn_{0.82}Zn_{0.21}Fe_{1.97}O$, $Mn_{0.70}Zn_{0.31}Fe_{1.99}O_4$, and $Mn_{0.62}Zn_{0.41}Fe_{1.97}O_4$. The X-ray diffraction and SQUID magnetometry were used to determine the spinel structure and ferrimagnetic properties of the samples. AC field heating experiments were performed on particles dispersed in glycerol to evaluate the specific absorption rate. Based on the superparamagnetic behaviour and magnetic hyperthermia data, the $Mn_{0.62}Zn_{0.41}Fe_{1.97}O_4$ phase was selected for further studies, including a more detailed characterization of the crystal and magnetic structure by neutron diffraction and Mössbauer spectroscopy, encapsulation into mesoporous silica, determination of the specific absorption rate of coated particles, and analysis of the porosity of the shell. Shortly, the $Mn_{0.62}Zn_{0.41}Fe_{1.97}O_4$ nanoparticles were found to possess high magnetization of M (10kOe) = 48.4 emu/g at room temperature and superparamagnetic behaviour at body temperature on the timescale of magnetic measurements. The coated product was formed by clusters of ferrite crystallites with overall mean size of 52 nm encapsulated into 22 nm thick mesoporous shell and showed heating efficiency of 57 W/g(Mn + Fe) in AC field of 970 kHz and amplitude of 8 mT. The mesoporous shell provided specific surface area of 670 m^2/g, and its pores of an average diameter 3 nm occupied specific volume of 0.45 cm^3/g. In a a preliminary study, the silica pores were loaded with rhodamine B as a model of a hydrophilic drug and subsequently enclosed by lauric acid that served as a temperature sensitive gatekeeper. The release of the model compound to aqueous medium was determined at room temperature and 60 °C by spectrophotometric analysis. Results have shown that amount of rhodamine B in pores achieved 15 mg per gram of silica-coated ferrite cores and its release was controlled by temperature.

1. Introduction

Magnetic nanoparticles have been prospected as suitable tools for various medical applications for decades, and among them iron oxide nanoparticles have been routinely used in clinical practice as negative contrast agents for magnetic resonance imaging (MRI) [1]. The iron oxide nanoparticles have been also employed, although in limited extent, for treatment of cancer by magnetic hyperthemia [2]. Magnetic nanoparticles are promising carriers for drugs, enabling active targeting by magnetic field, and such drug delivery systems can be combined with controlled release triggered by the heating effect in AC magnetic field. The strong therapeutic potential of magnetic nanoparticles can be accompanied by their employment for diagnostic purpose, such as visualization by means of MRI or magnetic particle imaging (MPI). In modern words, magnetic nanoparticles offer an excellent theranostic platform.

The nanoparticles for magnetically triggered release of drugs are designed as complex architectures, in which magnetic cores can be covered by a mesoporous shell that enables loading with drugs and functionalization with secondary thermoresponsive or thermosensitive coatings. These architectures, typically utilizing thermoresponsive copolymers based on *N*-isopropylacrylamide, and the release of drugs

* Corresponding author.
E-mail address: kamano@seznam.cz (O. Kaman).

https://doi.org/10.1016/j.jmmm.2018.11.020
Received 25 June 2018; Received in revised form 26 October 2018; Accepted 4 November 2018
Available online 05 November 2018
0304-8853/

triggered by an increase in temperature were already demonstrated years ago, see e.g. [3,4]. Another approach was demonstrated by application of suitable compounds as temperature-sensitive gatekeepers that enclose the pores [5,6]. Nevertheless, very little attention was paid to the magnetic cores of these complex particles.

Low toxicity, ease of preparation and historical reasons made the iron oxides the dominant type of magnetic nanoparticles in biomedical studies and in the development of theranostic particles. However, various spinel ferrites structurally related to magnetite but containing other metals as well, namely the $Mn_{1-x}Zn_xFe_2O_4$ or $Co_{1-x}Zn_xFe_2O_4$ compounds, offer an efficient control for optimal magnetic behaviour of the magnetic core with respect to specific requirements - in the given case to achieve high magnetization, high heating efficiency, superparamagnetic state on relevant timescale and high transverse relaxivity (see, e.g. Ref. [7] for comparison of the undoped Fe_3O_4 and its analogs $Zn_xFe_{3-x}O_4$ and $Mn_{1-x}Zn_xFe_2O_4$). As regards the surface modification of magnetic nanoparticles, mesoporous silica represents an attractive choice. First, silica is non-toxic, biologically inert and chemically stable, and its nanostructures form colloidally stable suspensions in water. Its mesoporous form possesses stable porous structure, which can be tuned with respect to the diameter of pores and geometry of their network [8]. Moreover, the silica surface enables facile anchoring of various organic moieties by covalent functionalization with complex silanes. Several methods were developed for controlled growth of mesoporous silica shells on metal oxide nanoparticles, most of which rely on tetraethyl orthosilicate (TEOS) as precursor of silica and application of suitable surfactants, such as cetyltrimethylammonium bromide (CTAB), or polymer templates as pore generating agents [9–11].

The present contribution considers Mn-Zn ferrite nanoparticles encapsulated into mesoporous silica as potential core material for theranostic systems that may combine the magnetically activated release of drugs and MRI tracking. Actually, small clusters of Mn-Zn ferrite nanoparticles were demonstrated to exhibit very high transverse relaxivity [12] and showed superior properties in detailed evaluation of their cytotoxicity compared to other promising contrast agents [13]. Specifically, the present study is devoted to hydrothermally prepared Mn-Zn ferrite nanoparticles of different compositions, whose magnetic behaviour and structure, including cation distribution, are thoroughly analysed. Importantly, their heating efficiency in AC magnetic fields is evaluated, and a suitable composition, namely $Mn_{0.6}Zn_{0.4}Fe_2O_4$ is selected based on magnetic and hyperthermia properties. These particles are coated with mesoporous silica shell, and the product is subjected to relevant characterizations including analysis of heating efficiency and porosimetry.

Finally, experiments on loading the mesoporous silica shell and heat-triggered release are performed by employing rhodamine B as a suitable model for hydrophilic drugs and lauric acid with melting point of 43 °C as the temperature-sensitive gatekeeper. In contrast to most of the previous studies, that typically tested rather hydrophobic compounds such as doxorubicin, paracetamol, etc. as model drugs, the present work is intentionally dedicated to hydrophilic compounds with high solubility in water, whose stable encapsulation into a drug delivery system combined with remotely triggered release poses clearly a difficulty.

2. Experimental details

2.1. Preparation of $Mn_{1-x}Zn_xFe_2O_4$ ferrite nanoparticles (MZF(x))

Stock solutions of manganese(II) nitrate, zinc nitrate, and iron(III) nitrate slightly acidified with nitric acid were used as starting materials. Their actual concentrations were determined by chelatometric titrations. Appropriate amounts were combined in the molar ratio Mn:Zn:Fe = (1 − y):y:1.80, where y = 0.20, 0.30, and 0.40, to reach the total metal content of 5.6 mmol. The resulting solution was concentrated in vacuo. Further, the solution was deoxygenated and transferred under inert atmosphere into a Berghof DAB-2 pressure vessel equipped with a 50 mL Teflon insert. Magnetic stirring was applied, and pH of the solution was adjusted to 10.0 by adding ≈2 M sodium hydroxide solution, which led to formation of brown precipitates. The so-obtained mixture was subjected to the hydrothermal treatment under autogenous pressure at 180 °C for 12 h. The filling volume was 50%, and magnetic stirring was applied during the whole synthesis. The product was washed several times with water and ethanol, and was dried on air.

2.2. Coating of $Mn_{0.62}Zn_{0.41}Fe_{1.97}O_4$ nanoparticles with mesoporous silica (MZF(0.41)@m-sil)

Bare MZF(0.41) nanoparticles (150 mg) were dispersed in 0.33 wt% aqueous solution of CTAB template (450 mL) in a 1 L round bottom flask equipped with a Teflon mechanical stirrer and placed in an ultrasound bath tempered to 50 °C. At first, both ultrasound agitation and mechanical stirring were applied. After 30 min, pH of the suspension was adjusted to 10–11 by ammonia (≈1 mL) and ethylacetate was added (15 mL). After 15 min, the silica precursor TEOS (2 mL) was added. The ultrasound agitation was terminated after additional 15 min. The temperature was kept at 50 °C for 4 h while mechanical stirring was applied. The particles were separated by centrifugation and washed with ethanol and water. Further, residual CTAB was removed from the raw product by ligand exchange procedure according to [14]. Specifically, the raw product was refluxed in ethanol solution of NH_4NO_3 (200 mg in 100 mL), and the particles were thoroughly washed with ethanol and water. Finally, simple size fractionation was carried out by differential centrifugation at 728 rcf for 15 min, after which the supernatant was collected as the final MZF(0.41)@m-sil product.

2.3. Characterizations

The phase purity of bare ferrite samples MZF(0.21), MZF(0.31) and MZF(0.41), their crystal structure and the mean size of crystallites, d_{XRD}, were determined by powder X-ray diffraction (XRD) with CuKα radiation. The diffraction patterns were recorded at room temperature on a Bruker D8 diffractometer and analysed by the Rietveld method in the FULLPROF program. The Thompson-Cox-Hastings pseudo-Voigt function was applied to resolve strain and size contributions to the line broadening, whereas the instrumental profile was determined based on a strain-free tungsten powder with crystallite size of 9.4 μm.

The actual metal ratio in bare ferrite samples was determined by X-ray fluorescence spectroscopy (XRF) measured on an AXIOS spectrometer.

The sample MZF(0.41) was subjected to a combined study by powder neutron diffraction and Mössbauer spectroscopy to analyse the low-temperature ferrimagnetic ordering and cation distribution over the tetrahedral and octahedral sites of the spinel structure. The neutron diffraction measurement was performed on a high resolution two-axis powder diffractometer at the Laboratoire Léon Brillouin in Saclay. The wavelength of 1.225 Å was applied, and the measurement was carried out at 2 K. The neutron diffraction pattern was also analysed by the Rietveld method in the FULLPROF program. The ^{57}Fe Mössbauer spectra were collected in transmission arrangement with a ^{57}Co/Rh source. The in-field spectra were acquired in external magnetic field of B_{ext} = 6 T at 4.2 K in a JANIS cryostat. Calibration of velocities and isomer shifts was based on α-Fe at 296 K.

Magnetic behaviour of nanoparticles was probed by SQUID magnetometry in DC fields by means of a Quantum Design MPMS XL system. The magnetization curves were measured up to the fields of 40 kOe at temperatures of 5 and 300 K. Susceptibility measurements were carried out in zero-field-cooled (ZFC) and field-cooled (FC) regimes by using the probe field of 20 Oe.

The morphology and size of MZF(0.41)@m-sil nanoparticles were studied by transmission electron microscopy (TEM) by using a Philips

CM 120 system. In addition, dynamic light scattering (DLS) was employed to determine the colloidal stability and hydrodynamic size of coated particles in water. The measurements were carried out at 25 °C on a Malvern Zetasizer Nano S. The porosimetric study of the coated product was carried out on a Micromeritics ASAP 2050 analyser to determine the specific surface area, distribution of pore sizes and specific volume of pores present in the coating. The coated particles were dried in vacuo at 40 °C, and nitrogen physisorption measurements were carried out at -196 °C. The specific surface area was evaluated by using the Brunauer-Emmett-Teller model. The pore size distribution was determined by the Barrett-Joyner-Halenda method, but the specific pore volume was calculated only based on the first component of the distribution with pore diameter up to 10 nm. Further, helium pycnometry was applied to determine the skeletal density of coated particles.

2.4. Magnetic heating experiments in AC field

Heating experiments in AC magnetic fields were carried out on a home-made system [15], where the temperature of a suspension was recorded as a function of time. Since bare ferrite nanoparticles do not form a colloidally stable aqueous suspension, the bare particles were measured in a form of dispersion in glycerol (50 mg of particles in 2.2 g of glycerol) in magnetic fields of various frequencies (54–960 kHz) and amplitudes (8–11.5 mT). Based on obtained results, coated nanoparticles of the ferrite with the largest Zn content and optimum superparamagnetic behaviour, MZF(0.41)@m-sil, were selected for a more detailed heating experiments on a colloidally stable aqueous suspension.

2.5. Loading and heat-triggered release of model compounds

The MZF(0.41)@m-sil particles were separated from the original aqueous suspension by centrifugation, redispersed in absolute ethanol and dried in vacuo at room temperature. The dry particles (2 mg) were dispersed in a solution of rhodamine B (2 mg) in absolute ethanol (0.5 mL) and agitated by ultrasound overnight. The ethanol was evaporated in vacuo, and lauric acid (115 mg) was added. The mixture was heated to 80 °C, shortly dispersed by ultrasound probe and further heated for 2 h. Upon addition of water tempered to 80 °C (1.6 mL), the mixture formed an emulsion. The lower aqueous phase containing hydrophilic particles was separated, while possible contamination by the upper oil layer was avoided. The particles were separated from the aqueous phase by centrifugation, and the corresponding supernatant with excessive rhodamine B was discarded. The particles were redispersed in water by short insertion in an ultrasound bath, and the resulting suspension was divided into two equal halves, whose volumes were adjusted to 1.8 mL.

One of the two samples obtained was incubated at room temperature for 20 min, whereas the other one was heated to 60 °C. Then both samples were centrifuged at 14,000 rpm for 15 min, supernatants were isolated for spectrophotometric analysis, and residues were dispersed in water (1.8 mL). The treatment at room and elevated temperatures were repeated until the respective supernatants were almost colourless. After the last treatment in water, the particles were redispersed in ethanol (1.8 mL) to dissolve lauric acid and release the residual rhodamine B. The ethanolic suspension was centrifuged again, and the supernatant was separated for analysis. The residue containing particles was quantitatively transferred to a small piece of a Teflon tape, dried slowly on a steam bath and subjected to SQUID magnetometry to determine the content of magnetic particles in both compared samples.

The concentration of rhodamine B in all supernatants was determined based on UV–Vis spectra recorded on a Shimadzu UV-1800 spectrophotometer. The absorbance was evaluated at the wavelength of the absorption maximum in water and ethanol, λ_{max} = 553 and 543 nm, respectively, considering carefully actual background of each sample.

Table 1
Selected properties of bare Mn-Zn ferrite nanoparticles: composition according to XRF, lattice parameter a, mean size of crystallites d_{XRD}, and the moment of spontaneous ordering, m, according to magnetometry at 5 K.

Sample	Composition	a [Å]	d_{XRD} [nm]	m [μ_B per f.u.]
MZF(0.21)	$Mn_{0.82}Zn_{0.21}Fe_{1.97}O_4$	8.4761(5)	14	4.31
MZF(0.31)	$Mn_{0.70}Zn_{0.31}Fe_{1.99}O_4$	8.4669(6)	13	4.34
MZF(0.41)	$Mn_{0.62}Zn_{0.41}Fe_{1.97}O_4$	8.4617(5)	12	4.17

3. Results and discussion

3.1. Characterizations of magnetic cores

According to XRD analysis, all of the three bare Mn-Zn ferrite samples were prepared as single-phase products with the spinel structure of the $Fd\bar{3}m$ symmetry and the mean crystallite size of $d_{XRD} \approx$ 13 nm. The actual chemical composition of the ferrites was accurately determined by XRF, which showed that the Mn:Zn ratio closely reflected the ratio of metals used in the reaction mixture. The data obtained are summarized in Table 1.

The combined study of MZF(0.41) nanoparticles by neutron diffraction and Mössbauer spectroscopy allowed to determine the cation occupancy to 24.7%Mn + 28.3%Zn + 47%Fe in the tetrahedral site and 18.6%Mn + 6.4%Zn + 75%Fe in the octahedral one, see [16] for details. This is a rather expected result, especially in view of strong preference of Zn^{2+} ions for tetrahedral coordination and tendency of Fe^{3+} ions for octahedral coordination in bulk spinels. The partially inverse location of Zn^{2+} should be ascribed to the non-equilibrium state of nanoparticles grown hydrothermally under the temperature as low as 180 °C. However, we may note that still larger octahedral occupancy of Zn^{2+} ions was reported for nanoparticles of $Co_{1-x}Zn_xFe_2O_4$ (x = 0.6 and 0.7, d_{XRD} = 13–17 nm) prepared by coprecipitation and annealing at 500 °C [17]. Another interesting finding to consider is the distribution of Zn^{2+} in $Mn_{0.7}Zn_{0.3}Fe_2O_4$ nanoparticles (size of 15 nm according to TEM) prepared by the thermal decomposition method at 300 °C, which was almost limited to tetrahedral sites according to EXAFS analysis [7]. These results suggest that the actual distribution of cations in nanoparticles with the spinel structure is rather determined by the preparation route than by the size of crystallites, and both the non-equilibrium and thermodynamically stable, bulk-like distributions can occur in nanocrystalline forms.

As the ferrimagnetic order is concerned, the neutron diffraction data at 2 K showed average moments at the tetrahedral and octahedral sites m_T = -3.30 μ_B and m_O = 3.47 μ_B, respectively, which yields a total magnetic moment of $|m| = 2|m_O| - |m_T|$ = 3.63 μ_B per formula unit. This means that magnetic cations Mn^{2+} and Fe^{3+} in tetrahedral sites contribute in average by 4.60 μ_B, which is close to their theoretical spin-only values of 5 μ_B and points thus to their practically parallel alignment. On the other hand, the contribution of the same cations in octahedral sites makes 3.70 μ_B only, which suggests that there is certain disorder due to competing FM and AFM interactions in the octahedral sublattice, leading to significant canting of individual spins from the ferrimagnetic axis.

3.2. Magnetic properties

The ZFC-FC susceptibility studies on bare Mn-Zn ferrite nanoparticles are presented in Fig. 1a. It is seen that ferrimagnetic ordering in the MZF(0.41), MZF(0.31) and MZF(0.21) particles occurs at temperatures higher than the experimental limit of the employed magnetometer set-up (400 K), i.e. well above the room temperature. Previous reports on the $Mn_{1-x}Zn_xFe_2O_4$ series showed that Curie temperatures systematically decrease with increasing Zn content, similarly for bulk

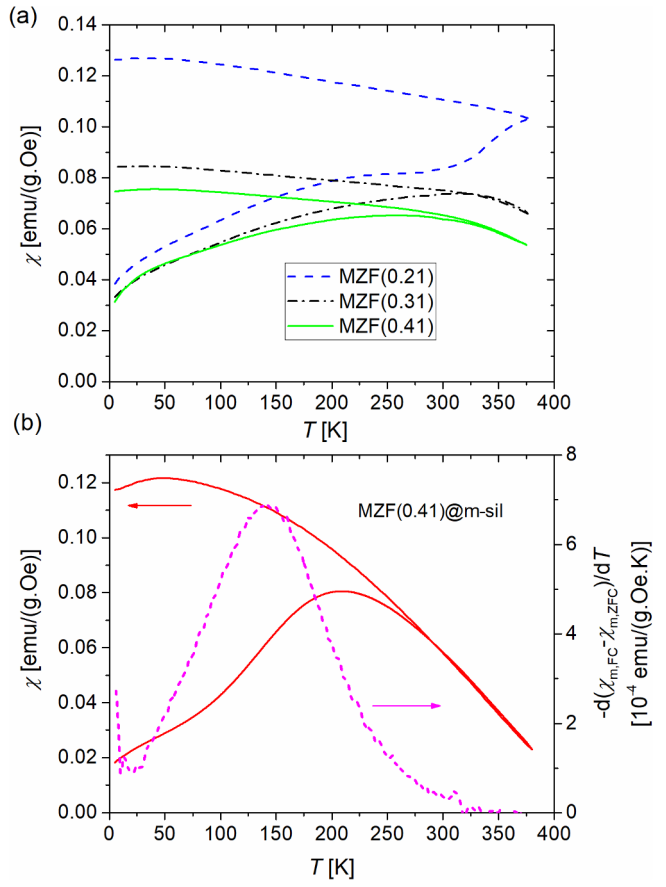

Fig. 1. ZFC-FC susceptibility studies in magnetic field of $H = 20$ Oe: (a) bare Mn-Zn ferrite nanoparticles of different composition, (b) MZF(0.41)@m-sil sample. The lower panel is supplemented with the temperature derivative of the FC-ZFC difference.

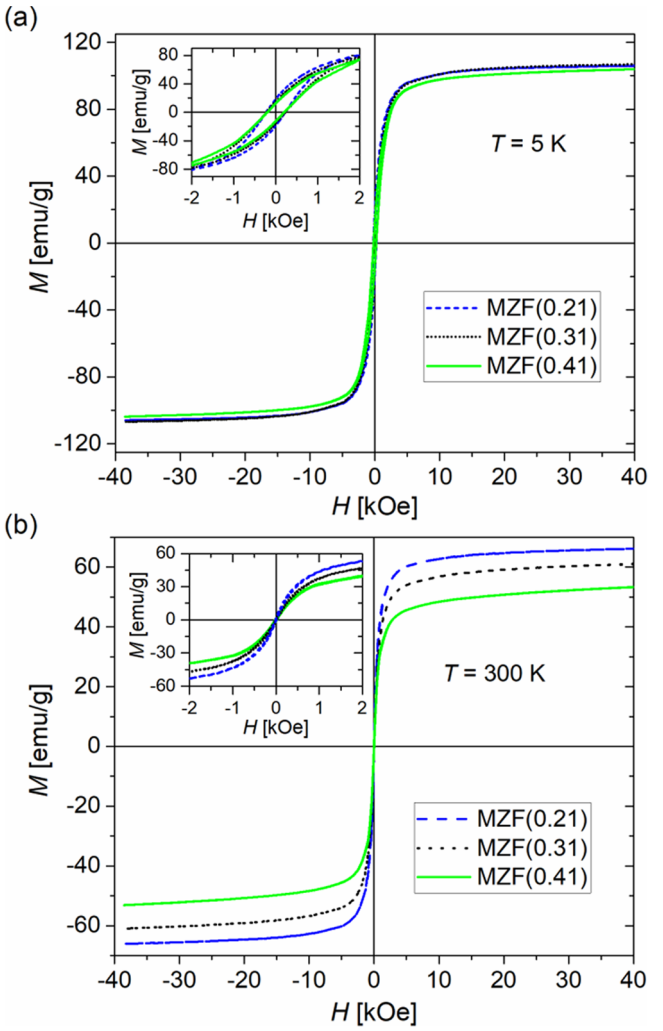

Fig. 2. Hysteresis loops of bare Mn-Zn ferrite nanoparticles at (a) low and (b) room temperatures.

and nanosize forms, see e.g. [18]. As regards the present samples, we can roughly estimate at least the Curie temperature of the phase with the highest zinc content, MZF(0.41), based on the temperature dependence of saturation magnetization, to $T_C \approx 425$ K.

Importantly, the ZFC-FC susceptibility studies provide insight into the blocking behaviour of magnetic nanoparticles. The systematic decrease in the temperature of the ZFC susceptibility maximum and the decrease in the irreversibility temperature (the temperature of the ZFC-FC bifurcation) with increasing zinc content indicate that the onset of the superparamagnetic state occurs at lower temperatures for samples with higher zinc content. However, the magnetic behaviour of bare particles is strongly affected by dipolar interparticle interactions that lead to blocking at lower temperatures (the effect of dipolar interactions on particle blocking is discussed in detail in [19]). These interactions are hindered in silica-coated particles, whose ZFC-FC studies are more relevant with respect to the anticipated application. The effect of diamagnetic coating is exemplified in Fig. 1b on the sample MZF(0.41)@m-sil, where clear shift of both the ZFC maximum and the irreversibility to lower temperatures (compared to the bare particles in Fig. 1a) is observed. The derivative of the ZFC-FC difference, also shown in Fig. 1b, describes the distribution of temperatures of particle blocking in MZF(0.41)@m-sil on the timescale of magnetic measurements [20]. Actually, the particular composition close to the $Mn_{0.6}Zn_{0.4}Fe_2O_4$ stoichiometry was selected for further studies since even the bare sample is almost completely superparamagnetic at body temperature and lacks any blocked fraction.

The magnetization curves of bare samples are presented in Fig. 2. The data at 5 K show rather high coercivity, $H_C = 200$–230 Oe (see Fig. 2a), which can be attributed to an effect of magnetic interactions among bare particles. The spontaneous magnetization presently observed at 5 K ranges between $M_s = 99.1$–103.7 emu/g, which corresponds to ferrimagnetic moments of $m = 4.17$–4.34 μ_B per formula unit, as summarized above in Table 1. For the samples MZF(0.41), the moment of spontaneous ordering of 4.17 μ_B per f. u. can be compared with the spontaneous moment determined by neutron diffraction of 3.63 μ_B per f. u. This may mean that the moments are lowered by about 10% when measured in the absence of external field, which suggests that some fraction of the finest particles could remain in the superparamagnetic state even at the lowest temperature. The room-temperature hysteresis curves of bare samples seem to be anhysteretic (see Fig. 2b), which can be explained either by superparamagnetic behaviour of the particles (the case of MZF(0.41)) or by a very low coercivity that is below the experimental limit of the measurement (due to remnant fields in the superconducting winding). Magnetization curves at room temperature approach quickly saturation, and the magnetization achieves 48.4–63.0 emu/g at 10 kOe. These values can be compared with magnetization of iron oxide nanoparticles prepared under comparable conditions, e.g. hydrothermal synthesis at 100–200 °C led to iron oxides with $d_{XRD} = 13$–23 nm and saturation magnetization of 27–34 emu/g [21].

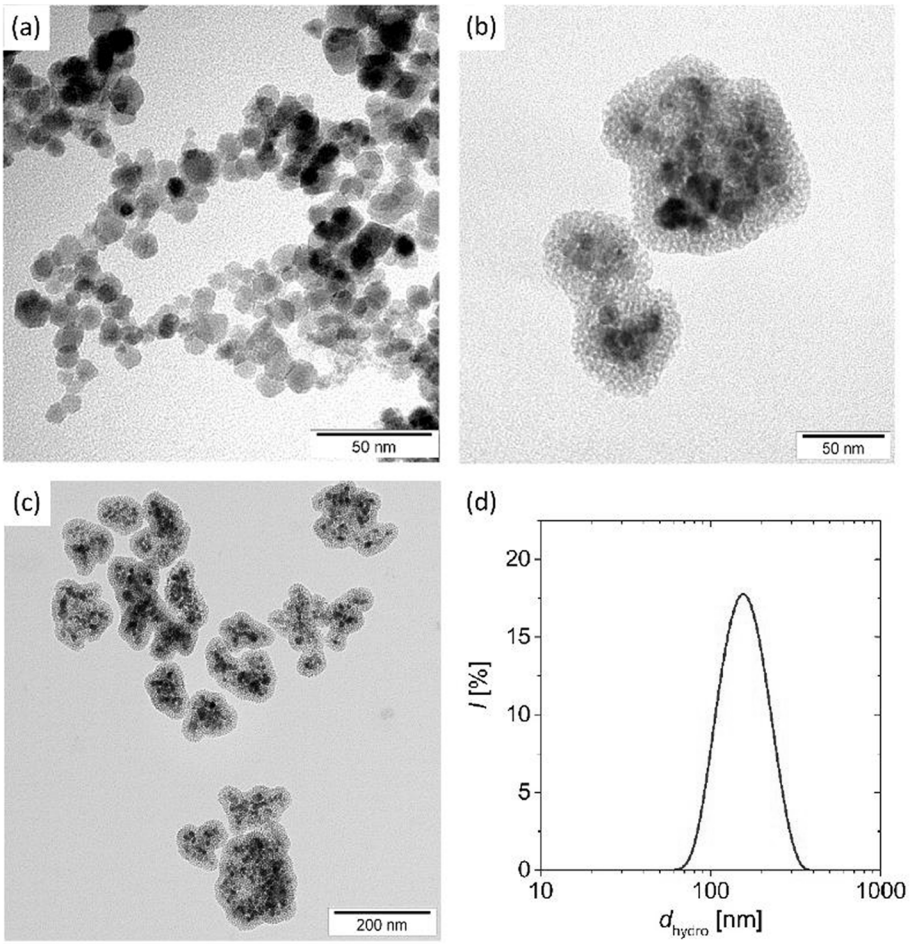

Fig. 3. Transmission electron micrographs of (a) bare MZF(0.41) and (b, c) coated MZF(0.41)@m-sil nanoparticles. (d) The intensity distribution of hydrodynamic size, d_{hydro}, of the coated sample in water.

3.3. Size, morphology and porosimetry of $Mn_{0.62}Zn_{0.41}Fe_{1.97}O_4$ coated with mesoporous silica

The TEM images of the bare MZF(0.41) and coated MZF(0.41)@m-sil nanoparticles are presented in Fig. 3a-c. The mesoporous silica makes a continuous coating, formed generally on small clusters of ≈10 nm ferrite crystallites. Detailed image analysis of micrographs provided data on the size distribution of whole coated particles d_p, their overall magnetic cores d_c, and also on the distribution of shell thickness e, see Fig. 4a,b. The mean size of the whole particles is $\bar{d}_p = 99$ nm with $\sigma_p = 15$ nm and the mean size of their magnetic cores is $\bar{d}_c = 52$ nm with $\sigma_c = 13$ nm, whereas the mean thickness of the mesoporous coating was evaluated to $\bar{e} = 22$ nm with $\sigma_e = 6$ nm.

Complementary data were obtained by DLS on aqueous suspension of MZF(0.41)@m-sil nanoparticles, which confirmed the colloidal stability in water and provided Z-average value of hydrodynamic size $d_Z = 150$ nm and polydispersity index $pdi = 0.069$. The rather broad intensity distribution of the hydrodynamic size is shown in Fig. 3d.

Further, a detailed study was devoted to the composition and porosity of the MZF(0.41)@m-sil sample. Taking into account that the coated sample showed magnetization of M(30kOe, 5 K) = 28.1 emu/g compared to the magnetization of bare MZF(0.41) particles of M (30kOe, 5 K) = 102.8 emu/g, the silica content in the coated product is estimated to 72.7 wt%. Further, the skeletal density of the sample was determined by helium pycnometry to 2.187 g/cm^3, which enables to evaluate the skeletal density of the mesoporous silica to 1.80 g/cm^3. The latter value can be compared with the tabulated value of 2.20 g/cm^3 for fused silica.

According to the nitrogen physisorption measurements, the mean diameter of mesopores was ≈3 nm (see the distribution in Fig. 4c), and their total volume was determined to 0.45 cm^3 per gram of coated particles. This allows us to calculate the volume fractions in the MZF (0.41)@m-sil particles to 6 vol% of ferrite cores, 45 vol% of silica phase and 49 vol% of pores, which means that volume of mesopores roughly equals to volume of their silica framework. Finally, the physisorption measurements evidenced also high specific surface area of MZF(0.41)@m-sil particles determined to 670 m^2 per gram of coated particles. When the pore volume and surface area are related to the weight content of silica only, we get the values of 0.62 cm^3/g and 920 m^2/g, respectively. These are close to the values of 0.77 cm^3/g and 1079 m^2/g, reported for a sample of pure mesoporous silica of the MCM-41 type prepared by employing the CTAB template and calcination at 823 K [22].

3.4. Heating in AC magnetic fields

The heating efficiency at ambient temperature was evaluated as the specific absorption rate

$SAR = \frac{C_p}{m(Fe+Mn)}\frac{dT}{dt}$, where C_p is the heat capacity of the suspension, m(Fe + Mn) is the mass of magnetically active elements and dT/dt is the initial slope of the dependence of temperature on time. The results for bare particles MZF(0.41), MZF(0.31) and MZF(0.21) in glycerol, presented in Table 2, do show rather minor variation, and it is not clear whether the differences arise from the different composition or minor differences in the size of particles. However, an increase in the heating efficiency with increasing frequency of the applied field is well obvious for all three samples. This increase is more pronounced for the

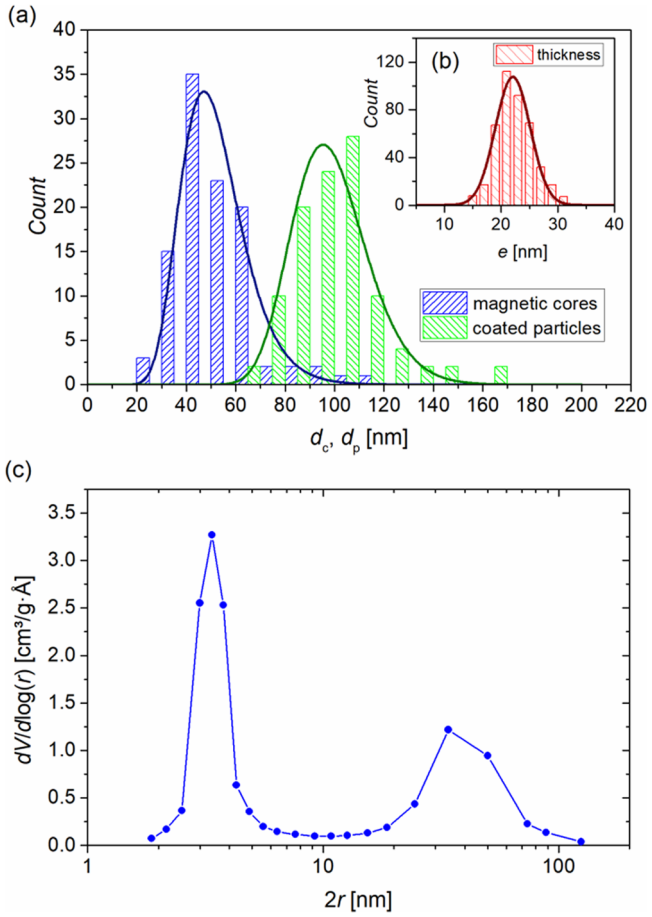

Fig. 4. Image analysis and porosimetry of MZF(0.41)@m-sil particles: (a) the size distribution of whole particles and the size distribution of their magnetic cores, including their log-normal fits, (b) the distribution of the mesoporous shell thickness *e*, (c) the distribution of the pore diameters (in logarithmic abscissa scale).

Table 2
SAR values [W/g(Fe + Mn)] determined on glycerol dispersions of bare Mn-Zn ferrite nanoparticles and on the aqueous suspension of coated MZF(0.41)@m-sil particles:

AC field	MZF(0.41)	MZF(0.31)	MZF(0.21)	MZF(0.41)@m-sil
485 kHz, 8 mT	28	34	27	39
108 kHz, 8 mT	6	10	10	7
54 kHz, 8 mT	3	4	7	3

composition MZF(0.41) than for the two others, which might be attributed to their different magnetic behaviours in AC fields. The Neél relaxation is likely to contribute only for MZF(0.41) particles, whereas heating effects of MZF(0.31) and MZF(0.21) should be discussed based on hysteresis losses of single domain particles. (The contribution of Brown relaxation and viscous losses is likely comparable for all three samples.) In the former case, the dependence of SAR on frequency, *f*, can be expressed through the product $f.\chi''(f)$, where $\chi''(f)$ is the imaginary part of susceptibility that forms a peak. In the latter case, the SAR is simply given by the hysteresis loss per cycle multiplied by the frequency [23].

In view of eventual development of efficient theranostic agents, it is desirable to use superparamagnetic particles with high magnetization, high transverse relaxivity (see the relaxometric data on hydrothermally prepared Mn-Zn ferrite nanoparticles in [13]) and reasonable heating efficiency. Among the present samples, the MZF(0.41) nanoparticles

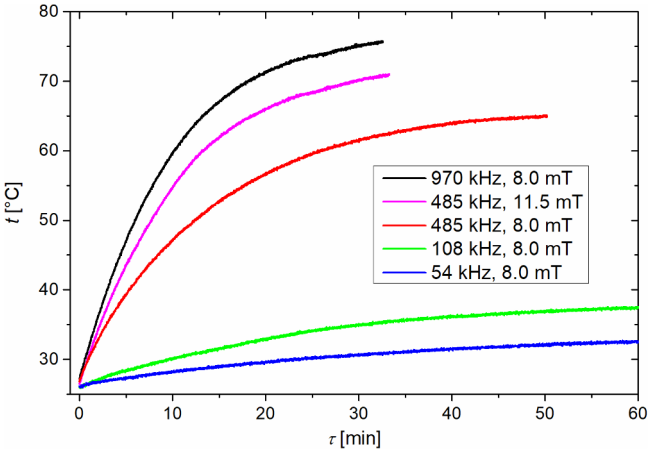

Fig. 5. Magnetic heating of MZF(0.41)@sil@m-sil nanoparticles at concentration of 10 mg(ferrite)/mL in various AC fields.

represent probably the best choice, and further experiments were thus directed to evaluation of heating efficiency of MZF(0.41)@m-sil in the form of colloidally stable suspension in water. The experiments are illustrated by the dependences of the suspension temperature on time in Fig. 5, and selected *SAR* values have been included in Table 2. One may note that *SAR* values observed for MZF(0.41)@m-sil particles in aqueous suspension are roughly comparable with *SAR* determined for bare MZF(0.41) particles in glycerol.

As regards the experiments depicted in Fig. 5, the AC magnetic heating of the coated particles in aqueous suspension increases steeply with increasing frequency and field amplitude, with highest *SAR* of 57 W/g(Mn + Fe) achieved at 970 kHz and 8 mT.

3.5. Loading and heat-triggered release of rhodamine B

Preliminary experiments with loading and heat-triggered release were inspired by the study of Liu et al. [5], who prepared maghemite nanoparticles coated with mesoporous silica and employed doxorubicin as a model drug and 1-tetradecanol with melting point of 38 °C as the temperature-sensitive gatekeeper. Our study was directed to the development of remotely controlled drug delivery systems for hydrophilic drugs, and thus rhodamine B, i.e chloride of an organic cation that shows high solubility in water, was selected as a model. At the same time, lauric acid with somewhat higher melting point seemed to be a reasonable choice of the gatekeeper.

The results of the spectrophotometric determination of rhodamine release from the studied system at room and elevated temperatures are shown in Fig. 6. The difference between the gradual release of rhodamine at given temperatures documents the temperature-controlled mechanism. Although leaching of rhodamine at room temperature is considerable, the data show that even hydrophilic compounds with high solubility in water can be encapsulated in such drug delivery systems and their release can be partially controlled by external physical stimuli.

The magnetic measurements of the samples involved in these experiments enabled to quantify the amount of ferrite phase and thus determine accurately the drug loading capacity. Specifically, the content of rhodamine B in particles capped by lauric acid was 15 mg per 1 g of the silica-coated ferrite, which relates to the sample obtained after the removal of free excessive rhodamine B present in the original emulsion.

4. Conclusions

The ≈100-nm sized particles build of clusters of 10-nm sized $Mn_{0.62}Zn_{0.41}Fe_{1.97}O_4$ ferrite crystallites and mesoporous silica shell are

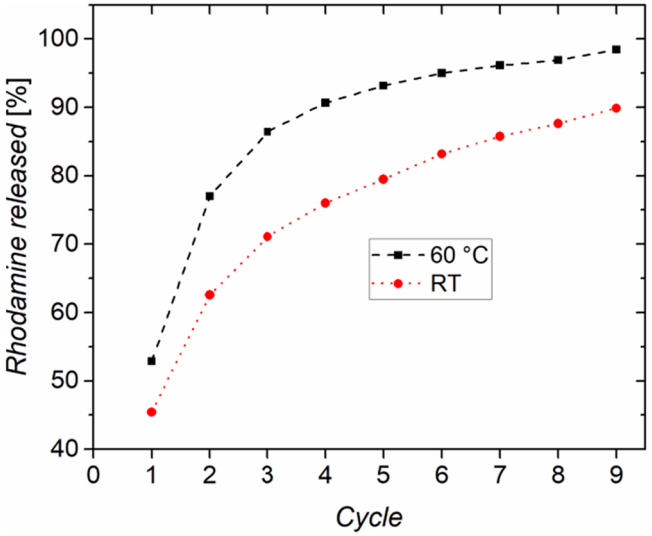

Fig. 6. Cumulative release of rhodamine B from particles MZF(0.41)@sil@m-sil that were loaded with rhodamine B and subsequently capped by lauric acid. In every cycle, one sample was incubated at 60 °C for 20 min while the other one was kept at room temperature (RT). Then both the samples were centrifuged and rhodamine B was determined spectrophotometrically in respective supernatants.

suggested as a suitable platform for drug delivery systems. Provided that the surface of the mesoporous shell is covered by a temperature-sensitive gatekeeper, the particles enable thermally controlled release of therapeutic agents that can be triggered, e.g. by the heating effect of the particles in an alternating magnetic field. Moreover, high magnetization of these particles would facilitate their tracking by MRI, i.e visualization of the drug delivery system during application.

In the model particles actually tested, the ferrite core amounted to 27 wt% of the coated particles and was formed by a small number of 10 nm nanocrystallites, making clusters of the mean size 52 nm. At room temperature, the magnetization of the given Mn-Zn ferrite crystallites was 48.4 emu/g at 10 kOe. The ferrite core was embedded in a 22 nm thick mesoporous silica shell, the framework of which comprised 52 vol% of pores with the mean diameter of 3 nm. Considering the whole coated particles, the specific volume of pores reached 0.45 cm^3/g and the specific surface area of the mesoporous silica shell was 670 m^2/g. The heating efficiency in the AC magnetic field of 8 mT amplitude and 970 Hz frequency amounted $SAR = 57$ W/g(Mn + Fe).

Finally, rhodamine B, selected as a model compound for hydrophilic drugs, was loaded into the mesoporous silica shell and subsequently stabilized by capping of particles with lauric acid as a temperature-sensitive gatekeeper. The resulting product was characterized by rhodamine content of 15 mg per 1 g of silica-coated ferrite, which means that there was roughly one molecule of rhodamine B per 24 nm^3 of the free pore volume. Although comparative experiments on the release of the model compound in aqueous media at room and elevated temperatures evidenced clear control by the temperature, the development of an efficient and remotely controlled delivery system for hydrophilic drugs remains challenging.

Further studies with respect to the ultimate goal, which is the preparation of robust thermoresponsive coatings and remote heating of functionalized particles through application of AC magnetic fields on their ferrite cores, are necessary.

Acknowledgements

The study was financially supported by the Czech Science Foundation under the project 16-04340S. Further, we would like to thank to Dr. Karel Soukup for the porosimetric measurements.

References

[1] S. Laurent, D. Forge, M. Port, A. Roch, C. Robic, L. Vander Elst, R.N. Muller, Magnetic iron oxide nanoparticles: synthesis, stabilization, vectorization, physicochemical characterizations, and biological applications, Chem. Rev. 108 (2008) 2064–2110, https://doi.org/10.1021/cr068445e.
[2] B. Thiesen, A. Jordan, Clinical applications of magnetic nanoparticles for hyperthermia, Int. J. Hyperther. 24 (2008) 467–474, https://doi.org/10.1080/02656730802104757.
[3] C.Y. Liu, J. Guo, W.L. Yang, J.H. Hu, C.C. Wang, S.K. Fu, Magnetic mesoporous silica microspheres with thermo-sensitive polymer shell for controlled drug release, J. Mater. Chem. 19 (2009) 4764–4770, https://doi.org/10.1039/b902985k.
[4] A. Baeza, E. Guisasola, E. Ruiz-Hernandez, M. Vallet-Regi, Magnetically triggered multidrug release by hybrid mesoporous silica nanoparticles, Chem. Mat. 24 (2012) 517–524, https://doi.org/10.1021/cm203000u.
[5] J. Liu, C. Detrembleur, M.-C. De Pauw-Gillet, S. Mornet, L.V. Elst, S. Laurent, C. Jérôme, E. Duguet, Heat-triggered drug release systems based on mesoporous silica nanoparticles filled with a maghemite core and phase-change molecules as gatekeepers, J. Mat. Chem. B 2 (2014) 59–70, https://doi.org/10.1039/c3tb21229g.
[6] I.-H. Cho, M.K. Shim, B. Jung, E.H. Jang, M.-J. Park, H.C. Kang, J.-H. Kim, Heat shock responsive drug delivery system based on mesoporous silica nanoparticles coated with temperature sensitive gatekeeper, Microporous Mesoporous Mat. 253 (2017) 96–101, https://doi.org/10.1016/j.micromeso.2017.06.042.
[7] J.T. Jang, H. Nah, J.H. Lee, S.H. Moon, M.G. Kim, J. Cheon, Critical Enhancements of MRI Contrast and Hyperthermic Effects by Dopant-Controlled Magnetic Nanoparticles, Angew. Chem. Int. Edit. 48 (2009) 1234–1238, https://doi.org/10.1002/anie.200805149.
[8] J.L. Slowing II, B.G. Vivero-Escoto, V.S.Y. Trewyn, Lin, Mesoporous silica nanoparticles: structural design and applications, J. Mater. Chem. 20 (2010) 7924–7937, https://doi.org/10.1039/c0jm00554a.
[9] G. Lelong, S. Bhattacharyya, S. Kline, T. Cacciaguerra, M.A. Gonzalez, M.L. Saboungi, Effect of surfactant concentration on the morphology and texture of MCM-41 materials, J. Phys. Chem. C 112 (2008) 10674–10680, https://doi.org/10.1021/jp800898n.
[10] A.B.D. Nandiyanto, S.-G. Kim, F. Iskandar, K. Okuyama, Synthesis of spherical mesoporous silica nanoparticles with nanometer-size controllable pores and outer diameters, Microporous Mesoporous Mat. 120 (2009) 447–453, https://doi.org/10.1016/j.micromeso.2008.12.019.
[11] C.T. Kresge, M.E. Leonowicz, W.J. Roth, J.C. Vartuli, J.S. Beck, Ordered mesoporous molecular-sieves synthesized by a liquid-crystal template mechanism, Nature 359 (1992) 710–712, https://doi.org/10.1038/359710a0.
[12] O. Kaman, J. Kuličková, V. Herynek, J. Koktan, M. Maryško, T. Dědourková, K. Knížek, Z. Jirák, Preparation of Mn-Zn ferrite nanoparticles and their silica-coated clusters: Magnetic properties and transverse relaxivity, J. Magn. Magn. Mater. 427 (2017) 251–257, https://doi.org/10.1016/j.jmmm.2016.10.095.
[13] O. Kaman, T. Dědourková, J. Koktan, J. Kuličková, M. Maryško, P. Veverka, R. Havelek, K. Královec, K. Turnovcová, P. Jendelová, A. Schröfel, L. Svoboda, Silica-coated manganite and Mn-based ferrite nanoparticles: a comparative study focused on cytotoxicity, J. Nanopart. Res. 18 (2016) 100, https://doi.org/10.1007/s11051-016-3402-5.
[14] N. Lang, A. Tuel, A fast and efficient ion-exchange procedure to remove surfactant molecules from MCM-41 materials, Chem. Mat. 16 (2004) 1961–1966, https://doi.org/10.1021/cm030633n.
[15] O. Kaman, P. Veverka, Z. Jirák, M. Maryško, K. Knížek, M. Veverka, P. Kašpar, M. Burian, V. Šepelák, E. Pollert, The magnetic and hyperthermia studies of bare and silica-coated $La_{0.75}Sr_{0.25}MnO_3$ nanoparticles, J. Nanopart. Res. 13 (2011) 1237–1252, https://doi.org/10.1007/s11051-010-0117-x.
[16] O. Kaman, D. Kubániová, L. Kubíčková, K. Knížek, J. Kohout, Z. Jirák, Ferrimagnetic ordering and cation distribution in hydrothermally prepared Mn-Zn ferrite nanoparticles, Unpublished results.
[17] M. Veverka, Z. Jirák, O. Kaman, K. Knížek, M. Maryško, E. Pollert, K. Závěta, A. Lančok, M. Dlouhá, S. Vratislav, Distribution of cations in nanosize and bulk Co-Zn ferrites, Nanotechnology 22 (2011) 345701, https://doi.org/10.1088/0957-4484/22/34/345701.
[18] N.T. Lan, T.D. Hien, N.P. Duong, D.V. Truong, Magnetic properties of $Mn_{1-x}Zn_xFe_2O_4$ ferrite nanoparticles prepared by using Co-precipitation, J. Korean Phys. Soc. 52 (2008) 1522–1525, https://doi.org/10.3938/jkps.52.1522.
[19] S. Bedanta, W. Kleemann, Supermagnetism, J. Phys. D-Appl. Phys. 42 (2009) 013001, 01300110.1088/0022-3727/42/1/013001.
[20] J.J. Lu, H.Y. Deng, H.L. Huang, Thermal relaxation of interacting fine magnetic particles - field-cooled and zero-field-cooled magnetization variation, J. Magn. Magn. Mater. 209 (2000) 37–41, https://doi.org/10.1016/s0304-8853(99)00640-x.
[21] S. Ahmadi, C.H. Chia, S. Zakaria, K. Saeedfar, N. Asim, Synthesis of Fe3O4 nanocrystals using hydrothermal approach, J. Magn. Magn. Mater. 324 (2012) 4147–4150, https://doi.org/10.1016/j.jmmm.2012.07.023.
[22] M. Grun, I. Lauer, K.K. Unger, The synthesis of micrometer- and submicrometer-size spheres of ordered mesoporous oxide MCM-41, Adv. Mater. 9 (1997) 254–257, https://doi.org/10.1002/adma.19970090317.
[23] R. Hergt, S. Dutz, Magnetic particle hyperthermia—biophysical limitations of a visionary tumour therapy, J. Magn. Magn. Mater. 311 (2007) 187–192, https://doi.org/10.1016/j.jmmm.2006.10.1156.